Transition to hard turbulence in thermal convection at infinite Prandtl number

Ulrich Hansen, David A. Yuen, and Sherri E. Kroening

Citation: Physics of Fluids A: Fluid Dynamics (1989-1993) **2**, 2157 (1990); doi: 10.1063/1.857802
View online: http://dx.doi.org/10.1063/1.857802
View Table of Contents: http://scitation.aip.org/content/aip/journal/pofa/2/12?ver=pdfcov
Published by the AIP Publishing

Articles you may be interested in

Internal heating driven convection at infinite Prandtl number
J. Math. Phys. **52**, 093101 (2011); 10.1063/1.3637032

Logarithmic bounds for infinite Prandtl number rotating convection
J. Math. Phys. **42**, 773 (2001); 10.1063/1.1336156

Characteristicsbased methods applied to infinite Prandtl number thermal convection in the hard turbulent regime
Phys. Fluids A **3**, 2105 (1991); 10.1063/1.857893

Mixing in the transition to strong turbulence in infinite Prandtl number thermal convection as applied to the Earth's mantle
Phys. Fluids A **3**, 1452 (1991); 10.1063/1.858039

Turbulent Thermal Convection at Arbitrary Prandtl Number
Phys. Fluids **5**, 1374 (1962); 10.1063/1.1706533

This article is copyrighted as indicated in the article. Reuse of AIP content is subject to the terms at: http://scitationnew.aip.org/termsconditions. Downloaded to IP: 169.237.93.46 On: Wed, 22 Oct 2014 15:53:15

Transition to hard turbulence in thermal convection at infinite Prandtl number

Ulrich Hansen
Institut für Geophysik, Universitat zu Köln, D-5000 Köln 41, Federal Republic of Germany

David A. Yuen and Sherri E. Kroening
Minnesota Supercomputer Institute and Department of Geology and Geophysics, University of Minnesota, Minneapolis, Minnesota 55415

(Received 27 February 1990; accepted 27 August 1990)

Direct numerical simulations of two-dimensional high Rayleigh (Ra) number, base-heated thermal convection in large aspect-ratio boxes are presented for infinite Prandtl number fluids, as applied to the Earth's mantle. A transition is characterized in the flow structures in the neighborhood of Ra between 10^7 and 10^8. These high Ra flows consist of large-scale cells with strong intermittent, boundary-layer instabilities. For Ra exceeding 10^7 it is found that the heat-transfer mechanism changes from one characterized by mushroom-like plumes to one consisting of disconnected ascending instabilities, which do not carry with them all the thermal anomaly from the bottom boundary layer. Plume–plume collisions become much more prominent in high Ra situations and have a tendency of generating a pulse-like behavior in the fixed plume. This type of instability represents a distinct mode of heat transfer in the hard turbulent regime. Predictions of this model can be used to address certain issues concerning the mode of time-dependent convection in the Earth's mantle.

I. INTRODUCTION

Recently the attention of scientists from various disciplines has been drawn to another transition in thermal convection. This transition, and the corresponding regime, called the regime of hard turbulence, has consequently been the subject of intense efforts involving laboratory experiments[1,2] and numerical simulations.[3] In all of these studies the different regimes are distinguished by means of the probability distribution of temperature fluctuations, exhibiting a change from a Gaussian to an exponential shape across this transition. However, in none of these studies, were the flow fields graphically displayed. In this work we will focus on the point of view of flow visualization in order to understand this phenomenon more physically. In what follows, we will present the evolution of the physical field for Rayleigh numbers between 5×10^5 and 10^8. Since we found it impossible to describe the full richness of the dynamics by words or single snapshots, we were motivated to use video movies as a means for visualization. A video containing the various cases shown in this paper is available from the authors.

Our investigation of convection at high Rayleigh numbers was motivated by the phenomenon of subsolidus mantle convection. For this reason we have focused on the infinite Prandtl number limit, which means that the flow can react instantaneously on any changes in the temperature field. For a long time it has been held by geophysicists that convection in the Earth's mantle prefers aspect ratios around unity and is essentially steady. Works by Machetel and Yuen[4] and Christensen[5] clearly demonstrated that time-dependent mantle convection can take place at Rayleigh numbers as low as 10^4 Hansen and Ebel[6] have shown that convection in fluids of infinite Prandtl number is "typically" time dependent at high Ra (about 10^6) and that the mode of this type of convection consists of a large-scale circulation with superimposed traveling thermal instabilities. Similar behavior was found in laboratory experiments by Krishnamurti and Howard[7] but for low Prandtl number fluids. It is this type of flow situation that has gained prominence in the problem of transition to hard turbulence in convection. The interaction of two scales of motion is believed to play a key role in this regard.[1,2] Understanding hard turbulence convection is of paramount interest for developing ideas about the dynamics of the interior of planets in their early epochs,[8] when there was large-scale melting.

The following simulations are two-dimensional in nature and one should therefore treat the results with some caution when extending to three-dimensional situations, as discussed by Goldhirsch *et al.*[9] Because our computational domain is two dimensional, we can extend the calculations to larger aspect-ratio configurations and explore many more cases than three-dimensional runs. Moreover, recent experiments by Solomon and Gollub[10] have borne out some of the features in plume dynamics, predicted by the two-dimensional calculations.

II. MODEL DESCRIPTION AND NUMERICAL METHODS

Infinite Prandtl number convection has been a topic of intense interest among geophysicists because of its application to mantle convection. The dimensionless equations representing infinite-Prandtl number, two-dimensional Boussinesq thermal convection in terms of streamfunction ψ and temperature T are given by

$$\nabla^4\psi = \mathrm{Ra}\,\frac{\partial T}{\partial x}, \tag{1}$$

$$\frac{\partial T}{\partial t} = \nabla^2 T + \frac{\partial \psi}{\partial x}\frac{\partial T}{\partial z} - \frac{\partial \psi}{\partial z}\frac{\partial T}{\partial x}, \tag{2}$$

where Ra is the thermal Rayleigh number. The dimensionless time is denoted by t, nondimensionalized by the thermal time across the layer depth d. The horizontal and vertical

 0899-8213/90/122157-07$02.00 © 1990 American Institute of Physics

This article is copyrighted as indicated in the article. Reuse of AIP content is subject to the terms at: http://scitationnew.aip.org/termsconditions. Downloaded to IP: 169.237.93.46 On: Wed, 22 Oct 2014 15:53:15

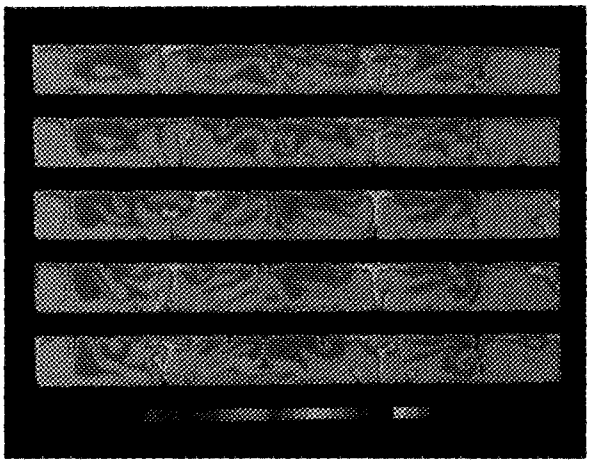

FIG. 1. Temperature fields at late stages for Ra = 10^6. Linear mapping of normalized temperature from purple ($T = 0$, top temperature) to red ($T = 1$, bottom temperature). Contour interval is 0.05. Free-slip boundaries, reflecting sides, constant temperature top and bottom: 31×300 elements were employed.

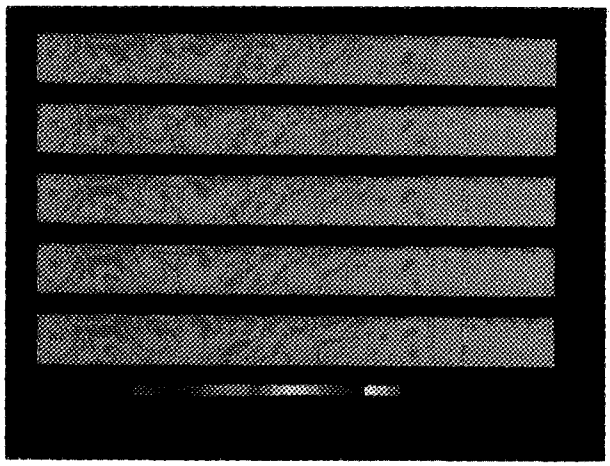

FIG. 3. Temperature fields at late stages for Ra = 10^8. Same convention as in Fig. 1. Here, 51×500 elements were employed. Higher resolution with 71×251 elements were used as higher resolution check for Ra = 10^8 and aspect ratio of 1.8. Recently this 1.8 aspect-ratio result has been checked with another method involving bicubic splines. We have used a 140×400 spline grid to verify the 71×251 elements.

coordinates are denoted by x and z, with the gravity vector g aligned opposite to z. We will solve Eqs. (1) and (2) with stress-free impermeable boundaries for all sides and reflecting boundary conditions (zero horizontal heat flux) at both edges. Stress free boundary conditions at the top and bottom are appropriate in describing mantle convection.[11] We have imposed constant temperatures at the top and bottom ($T = 1$ at $z = 0$, $T = 0$ at $z = 1$), which are consistent with the top and bottom thermal conditions of the mantle. Additional details can be found in Hansen and Ebel.[6]

We have employed a finite-element method, combined with an implicit, predictor–corrector time-stepping scheme, which is second-order correct, to solve the evolutionary equation. The biharmonic equation is solved directly by a variational principle at each time step with a maximum of 0.5 for the Courant criterion. The relative ease with which each local grid refinements can be implemented, makes the finite-element method well suited for the treatment of thin boundary layers. In a recent benchmark effort[12] the superiority of schemes using local grid refinement was illustrated. We have employed the Petrov–Galerkin method (e.g., Hughes[13]) for treating the thermal advection term. This leads to a local upwind scheme, which is efficient in tracking thermal fronts associated with plumes. A more-detailed description of this method can be found in Hansen and Ebel.[6]

Our aim of studying high Rayleigh number convection in large aspect-ratio boxes and of visualizing the time-dependent results brings about several technical difficulties in computation. First, an adequate resolution of the boundary-layer instabilities requires substantial amount of computational resources. For example, in our aspect-ratio ten box runs (see Figs. 1–4), we have used up to 510×51 elements, resulting in about 10^5 unknowns per time step and each run goes up to around 10^5 time steps. Second, visualization of fluid dynamical phenomena has become an important component of numerical modeling,[14] since we are interested in understanding the complete physical fields everywhere instead of specific output values, such as the horizontally averaged surface heat flux. Visualization also requires the man-

FIG. 2. Temperature fields at late stages for Ra = 2×10^7. Same symbols as in Fig. 1. Both 31×300 and 51×500 elements were used. No noticeable differences between the two grid configurations for this Ra.

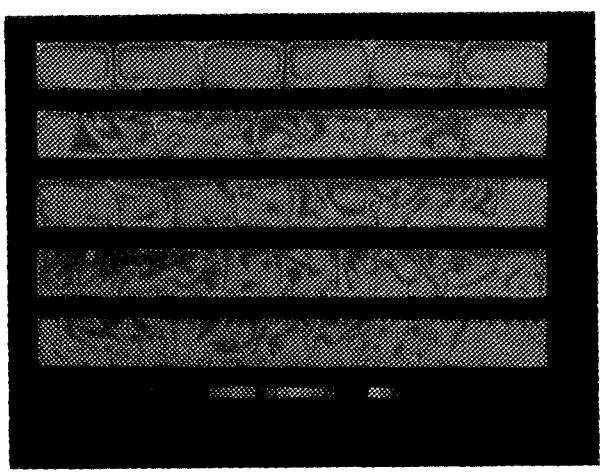

FIG. 4. Summary of temperature fields for a range of Ra. Going down, Ra is 5×10^5, 1×10^6, 5×10^6, 2×10^7, and 10^8. Note change between 5×10^6 and 2×10^7 and the sharper transition between 5×10^6 and 10^8.

This article is copyrighted as indicated in the article. Reuse of AIP content is subject to the terms at: http://scitationnew.aip.org/termsconditions. Downloaded to IP: 169.237.93.46 On: Wed, 22 Oct 2014 15:53:15

agement of an enormous amount of data. We have made videos of the runs, each containing around 5000 frames, because this represents a handy medium for demonstrating and also for discovering the richness of the dynamics of the flow. The color figures in the next section are snapshots taken from the video movies. But we emphasize that viewing the movies provides a much deeper understanding of the complex phenomena than just a few static figures.

III. RESULTS OF NUMERICAL EXPERIMENTS

In this section we present a series of calculations at Rayleigh numbers ranging from 5×10^5–10^8, because we are interested in the transition from weak to strong turbulence in high Prandtl number convection. The Rayleigh (Ra) number of the Earth's mantle may range between 5×10^5 and 10^8, depending on estimates of the lower-mantle viscosity, which is not well constrained at present. Previous works[5,6] have shown that the choice of a square box as a computational domain severely restricts the degree of freedom in the fluid system and hence inhibits the tendency of time-dependent flows to evolve. We have, therefore, chosen a box with an aspect ratio 10 in order to obtain the full richness of the dynamics in high Ra convection. Previous work on large box (aspect ratio of 12)[15] dealt with relatively low Ra, less than 10^6, and did not find any transition to large-scale circulation. Another motivation for investigating large aspect-ratio domains are the laboratory experiments performed by Krishnamurti and Howard[7] and numerical studies,[16] pointing to the existence of large-scale flows at high Ra. In laboratory experiments both the top and the bottom were kept at constant temperatures with rigid boundary conditions for all sides. Recently these large-scale coherent flows have revived the interests of workers on the new topic of transition to hard turbulence.[1]

In Fig. 1 snapshots, show the evolution of the flow at $Ra = 10^6$, similar to the results reported in Ref. 7. These solutions have already been integrated for at least 15 overturns, starting from a quasisteady solution obtained with a steady-state code. This initial condition in the temperature field is initially asymmetric in both directions. Convection does not take place in a strictly cellular mode and the flow is unsymmetric. Thermals are emanating from the hot and cold boundary layers that are superimposed on a circulation with a large scale. An opposite flow direction at the bottom and the top is the consequence of the large-scale circulation, causing strong deflections of the boundary layer instabilities. Besides the work of Krishnamurti and Howard[7] the coexistence of the two scales of motion has been observed in recent experimental efforts.[1,2,10] One important outcome of these works on laboratory convection was, that the interaction of the different scales plays a key role for the transition to the hard turbulence regime.

The first question one may ask is, what is the largest scale of the motion? the term "aspect ratio" has therefore lost its meaning and must be regarded at as a temporarily defined value. However, a "quasistable" circulation is driven by strong sinking and rising currents after many overturn times. For $Ra = 10^6$, flows of aspect ratios up to about 3 are maintained temporarily in the spin-up stage, although many smaller cells can exist simultaneously in the box. Previous work (Hansen and Ebel, Ref. 16) has shown that with increasing Ra the scale of the dominant cell, which can be maintained, is also growing. Extrapolating this result to very high Rayleigh numbers, we arrive at the same finding as the Krishnamurti and Howard experimental studies. That is, the largest scale of the flow is comparable to the width of the layer.

The small-scale flow—thermals or plumes—is generated by the instabilities within the thermal boundary layers. The classical boundary-layer theory[17] cannot provide a full description of the associated phenomena, since the existence of the large-scale circulation and the nonlinear interactions between the top and bottom boundary layers are simply neglected. Castaing *et al.*[2] addressed the issue concerning the evolution of such instabilities to the change of the large-scale circulation, which they coined the term "the wind" in their experiments in which no-slip velocity conditions were applied on all sides. In the following, we shall denote the term large circulation by L.S.C. In a numerical study Sirovich *et al.*[3] using stress-free boundary conditions for the top and bottom and periodic boundary conditions in the horizontal directions, did not find indications for the existence of the "wind" being sustained over a long time scale. However, over intermediate time scales such winds were found in their runs.[18] They proposed an accumulation of hot or cold blobs as a possible mechanism to form the plumes. Because of the large aspect ratio, L.S.C. influences the evolution of the thermals resulting from the longer exposure time. However, we cannot determine if the wind is the triggering mechanism for the small-scale instabilities, as proposed by Castaing *et al.*[2] The instabilities can likewise come from the thermal boundary layer, when a certain critical thickness is exceeded. At this stage the question, the extent to which the stability of the boundary layer depends on the delicate dynamical equilibrium between the L.S.C. and local boundary instability, remains open.[10]

The fate of these instabilities is ultimately determined by the L.S.C. There appears to be two ways for the thermals to reach the opposite boundary. One is to travel with the L.S.C. until they meet an already existing plume (two of these hot plumes can be seen in Fig. 1). These colliding plumes, trapping the traveling instabilities, are the driving mechanism for the "quasistable" large-scale circulation. Typically such "master plumes" are only slightly tilted and exhibit a pulse-like behavior, reflecting the capture of the "traveling slave instabilities." If the instabilities grow to a certain size before they meet a plume, they are then exposed to the "wind." This exposure results in a strong shear deformation of the thermal and often leads to a breakup, which has been observed in laboratory experiments.[19] Observe the sinking instabilities in Fig. 1. Increasing the Ra to 2×10^7 does not change the overall picture of the two-scale flow (Fig. 2). However, it does change the character of the individual plumes. Besides becoming narrower, as to be expected from boundary-layer theory, the plume cannot carry hot (from the lower boundary) or cold (from the upper) over as large a distance. Comparing to Fig. 1, deeply red or blue (i.e., hot or cold) regions

This article is copyrighted as indicated in the article. Reuse of AIP content is subject to the terms at: http://scitationnew.aip.org/termsconditions. Downloaded to IP: 169.237.93.46 On: Wed, 22 Oct 2014 15:53:15

are much more localized and can only be found in areas directly adjacent to the thermal boundary layers. Collisions of two or even more plume instabilities take place (for example, three instabilities meet in the hot plume in the right part of Fig. 2) resulting in an amplified outburst of the merged plumes out of the boundary layer. Similar to the thermal boundary layers, the thickness of the region, where the temperature of the thermals is significantly different from the cell interior, seems to decrease with further increasing Ra. This is an indication of greater mixing of the thermal anomalies with larger Ra. This phenomenon is demonstrated in Fig. 3, displaying snapshots of a run at $\mathrm{Ra} = 10^8$. Grid refinement has been used at both horizontal layers in order to capture the boundary-layer dynamics. The layer resembles to some extent the region, called the "mixing layer" in Castaing *et al.*[2] in the sense that instabilities, growing from the underlying boundary layer, are accelerated to the speed of the interior flow. Within this region the heat transport is governed by the small traveling instabilities, as also described in Sirovich *et al.*[3] Another noteworthy phenomenon occurring at this high Ra is the breakdown of most of the plumes, unlike the case of $\mathrm{Ra} = 10^6$ (Fig. 1), the plumes are not connected from the bottom to the top (or vice versa) but are forming disconnected "pod-like" structures. Sano *et al.*[1] gave a quantitative interpretation of this behavior in terms of the ratio $R = \tau_{\mathrm{diff}}/\tau_{\mathrm{conv}}$, where $\tau_{\mathrm{diff}} = \Delta^2/\kappa$ (Δ is the thickness of the boundary layer and κ is the thermal diffusivity) gives the characteristic time scale of the thermal boundary layer and τ_{conv} measures the "passage time"[1] of the L.S.C. They argued that a sufficiently small ratio of R would lead to a disconnection of the plumes. From their experiments they obtained a sharp drop of this ratio at Ra greater than about 10^7, thus providing an excellent explanation for the plume disconnections appearing in our simulations. We are not able to determine the exact Ra at which the transition occurs. However, it is clear that another discrete transition takes place somewhere between 10^7 and 10^8. Sano *et al.*[1] regarded the disconnection of the plumes as a possible mechanism for the transition from soft to hard turbulence. On this basis our numerical experiments indeed display the characteristics of the transition.

Figure 4 displays the late stages of the simulations at Ra ranging from 5×10^5 to 10^8. We observe clearly the transition from a regular, quasisteady state, cellular pattern to a strongly, time-dependent, two-scale flow in this range of Ra, spanning more than two orders in magnitude. We note that previously most of the simulations in geophysics have generally been done for Ra between 10^5 and 10^6 for large aspect-ratio boxes (e.g., Gurnis, Ref. 20). The cellular mode disappears more and more with increasing Ra and is replaced by irregularly distributed thermals. The large-scale circulation is still maintained but has a more temporal rather than a steady character. In order to verify the numerical resolution at $\mathrm{Ra} = 10^8$, we have employed a denser unevenly spaced grid of 71 (vertical) $\times$ 251 (horizontal) elements for an aspect-ratio 1.8 box. We have confirmed at $\mathrm{Ra} = 10^8$ the phenomenon of disconnected plumes for this higher resolution calculation by integrating over several overturns. Recently we have further confirmed these results with a bicubic spline method (Malevsky and Yuen[21]) in which a 140×400 grid was employed. This establishes the numerical integrity of these high Ra solutions.

Figure 5 shows the contoured horizontal-velocity fields at $\mathrm{Ra} = 10^6$ for three instants of time in the late stages. The arrows denote the borders of the large-scale cells, i.e., the zero crossings of the surface horizontal velocity. One can observe the presence of many cells with large aspect ratios, exceeding 2. In order to better monitor the evolution of the large-scale structure we have plotted the trajectories of the zero crossings $Z_i(x,t)$ as a function of time for $\mathrm{Ra} = 10^6$ [Fig. 6(a)] and $\mathrm{Ra} = 10^8$ [Fig. 6(b)]. In the case of $\mathrm{Ra} = 10^6$ we observe a pattern involving six large-scale cells with different aspect ratios, ranging from 0.8 to 2.5. In spite of the strong temporal fluctuations of Nu (not shown here) associated with the boundary-layer instabilities, the overall spatial structure seems to be almost invariant with respect to the scale of the cells. This phenomenon is due to the stably anchored "master plumes," discussed earlier. Within each cell the "wind" drives the boundary-layer instabilities around, thus generating the coherent flow pattern. As Ra is increased to 10^8, the cellular mode disappears, as shown clearly by Fig. 6(b). For the short time interval in the late stages displayed in Fig. 6(b), some boundary-layer instabilities remain relatively fixed, giving rise to the straight lines shown in the figure. The fluctuating trajectories arise from the collisions of the sinking blobs before they are detached from the top boundary layer. Unlike the $\mathrm{Ra} = 10^6$ case, in which traveling blobs are trapped by long-lasting up- or downwellings, the instabilities in this high Ra regime disappear via a "pulse-like" eruption after the collision of the plumes (denoted in Fig. 6 by the disappearance of the loops with time). Recent laboratory work by Solomon and Gollub[10]) showed such type of "pulse-like" eruptions of the boundary layer and they demonstrated by visualization the merging of boundary-layer instabilities, reminiscent of the "thermal-attractor" mechanism proposed by Vincent and Yuen.[22]

The Nusselt number, a measure of the global heat transport efficiency, is now no longer a function of the Ra alone, but is strongly time dependent. Fluctuations of Nu are due to the evolving boundary-layer instabilities and also due to the

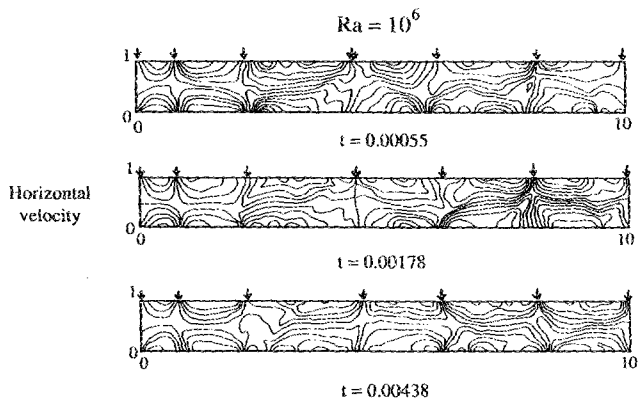

FIG. 5. Contour plots of the horizontal velocity field at $\mathrm{Ra} = 10^6$. Zero crossings of the horizontal velocity at the surface are marked by arrows.

This article is copyrighted as indicated in the article. Reuse of AIP content is subject to the terms at: http://scitationnew.aip.org/termsconditions. Downloaded to IP: 169.237.92.46 On: Wed, 22 Oct 2014 15:53:15

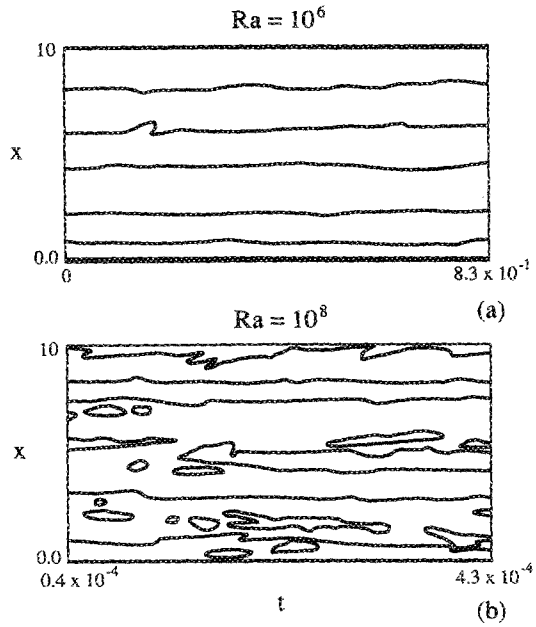

FIG. 6. (a) Zero crossings $Z_i(t,x)$ of the horizontal velocity at the surface ($z = 1$) as a function of time for Ra = 10^6. (b) Zero crossings $Z_i(t,x)$ on the surface as a function of time for Ra = 10^8. Otherwise, same as for (a).

reorganizations in the L.S.C. In general, variations of Nu that are caused by the latter mechanism operate on a much longer time scale and exhibit a higher amplitude than those associated with boundary-layer instabilities. The dependence of Nu on the aspect ratio of the steady-state L.S.C. has been reported earlier for two-dimensional, infinite Prandtl number convection. Nevertheless, the time-dependent effects caused by large reorganizations of the L.S.C. have been overlooked in the past, since many authors restricted themselves to small aspect-ratio domains where such reorganizations were almost excluded. It has been shown that such small aspect-ratio domains do not reflect typical time-dependent convection.[6]

For the average values of the Nusselt numbers, taken from the late stages of the simulations, we found the following:

$\mathrm{Ra} = 5\times10^5$	$\mathrm{Nu} = 14.5$
10^6	16.6
5×10^6	27.0
2×10^7	39.0
10^8	66.0.

All of these Nu's still exhibit fluctuations of about 10%. Obviously, even the maximum values of Nu are lower than those predicted from boundary-layer theory or from steady-state numerical calculations. Especially for high Rayleigh numbers, we found the discrepancies to be quire large. For two-dimensional infinite Prandtl number convection, Christensen[22] reported a value of Nu of about 95 for a steady-state flow in a square box at Ra = 10^8, which is about 20% higher than the average Nu from our calculations. The main reason for this discrepancy is that the aspect ratio of the different large-scale circulation systems is generally greater than unity. Thus, the heat transport associated with the L.S.C. is greatly reduced, as compared to the square box values.[16] Laboratory studies[1,2] have shown that not only the actual value of Nu, but also the functional dependence of the Rayleigh number, is altered by the transition to hard turbulence. Instead of the well-known $\mathrm{Ra}^{1/3}$ law, they found a dependence of the form $\mathrm{Nu}\sim\mathrm{Ra}^{2/7}$ appropriate for describing the heat transfer in the hard turbulent regime. From an experimental point of view, the Nu vs Ra relationship is much easier to measure than from numerical experiments, since many long runs would be involved in such a systematic study.

A possible explanation, which can be extracted from our simulations, is that the disconnected plumes are less efficient in the heat transport, thus leading to a decrease of the exponent. The hot or cold pieces left over from a disintegrating plume can easily be mixed in the cell's interior. This prevents a substantial amount of the heat from being transported to the top boundary.

In order to study the "carrying capacity" of these instabilities, we have monitored the maximum temperature as a function of the Ra number at different depth levels. Differing from the foregoing examples, we have used a domain of aspect ratio 1.8 instead of 10. Besides reducing the computational costs, we wanted to exclude the reorganizations of the flow (i.e., from one to two cells), which would have complicated the analyses. In Fig. 7 the maximum temperatures, taken from these experiments, are plotted versus Ra at three

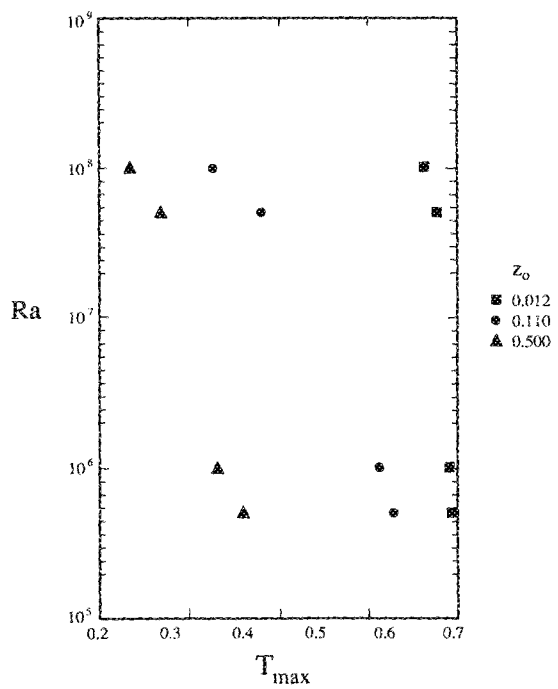

FIG. 7. Plot of Ra vs T_{max} at three different heights z_0. Here, $z_0 = 0.012$ is situated near the bottom, and 0.5 is in the middle. Aspect ratio of box is 1.8 and temperatures are taken at late stages.

This article is copyrighted as indicated in the article. Reuse of AIP content is subject to the terms at: http://scitationnew.aip.org/termsconditions. Downloaded to IP: 169.237.93.46 On: Wed, 22 Oct 2014 15:53:15

different depth levels ($z_0 = 0.012$, squares; $z_0 = 0.11$, circles; $z_0 = 0.5$, triangles). At $z_0 = 0.012$ we obtained very similar values for T_{max} at all four Ra's. This reflects that this position is within (for $Ra = 5 \times 10^5$ and 10^6) or immediately adjacent to the thermal boundary layer. The thermals are nearly unperturbed by the L.S.C. at this depth level. The picture changes at depth of $z_0 = 0.11$. Here, T_{max} has now become a monotonically decreasing function of Ra. At $z = 0.5$ the same trend exists. The maximum temperature that we found at $Ra = 10^8$ at this depth was $T_{max} = 0.63$, compared to $T_{max} = 0.76$ at $Ra = 5 \times 10^5$. Vigorous convection leads apparently to enhanced mixing of the boundary-layer instability and so to a more rapid cooling (or heating) of the plumes. Both mechanisms, the disconnection of the plumes and the bending and eventual breaking of the thermals by the L.S.C., serve to enhance the mixing, as compared to localized rising or sinking plumes.

The sinking instabilities should, of course, behave in the same way, i.e., with increasing Ra one would expect less pronounced (i.e., warmer) sinking instabilities. The combined effect of T_{max} and T_{min} are shown in Fig. 8 where the maximum temperature fluctuations ($T_{max} - T_{min}$) have been plotted versus Ra. With the exception of $z_0 = 0.012$ we find the expected behavior. Thus the fluctuation (0.29) at $z_0 = 0.5$ and $Ra = 10^8$ is smaller by a factor of 1.8 than the fluctuation at the same depth level at $Ra = 5 \times 10^5$. The increase of temperature fluctuation with Ra at $z_0 = 0.012$ is due to the fact that this sampling point is within the thermal boundary layer at the two lower Ra's and outside for both of the higher values. Generally speaking, the decreasing fluctuations argue for a reduced importance of the vertical motions or in other words: strong horizontal temperature gradients will not be maintained at high Ra convection in most parts of the cell.

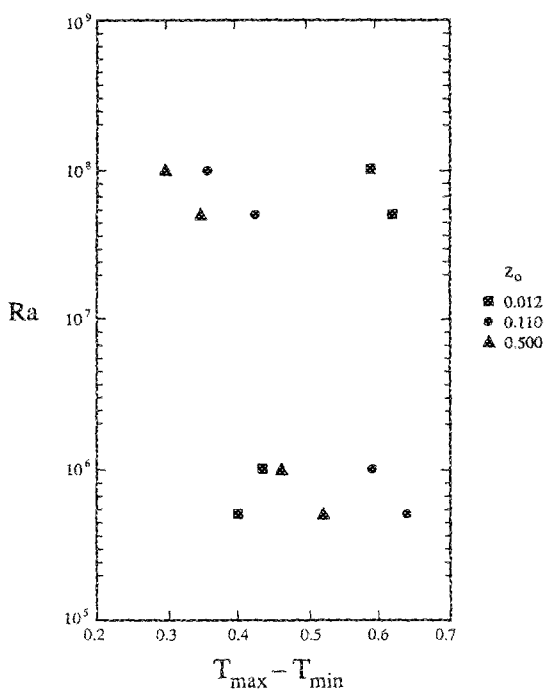

FIG. 8. Plot of Ra vs t_{min} at different heights z_0. Same convection as in Fig. 5. Note nonmonotonic behavior of $z_0 = 0.0123$. This is due to the width $\Delta z = 0.012$ being thinner than the boundary layers associated with Ra up to 10^6.

IV. DISCUSSIONS AND CONCLUDING REMARKS

The main merit of the above numerical experiments may be the relative ease of obtaining animations of the physical fields, thus providing the opportunity to understand intuitively the physics of the transition to hard turbulence. In this respect our two-dimensional work is complementary to the three-dimensional efforts by Sano *et al.*,[1] Castaing *et al.*[2] and Sirovich *et al.*,[3] since we are able to conduct a wider sweep of the parameter space in Ra and aspect ratios. It is also interesting in the sense that we have investigated an infinite Prandtl number fluid. One needs of course to extend these calculations to three-dimensional situations at high Ra, in order to confirm these two-dimensional findings. So far the experiments have been conducted at virtually constant Prandtl number (0.65–1.5) (papers listed above) and therefore only little is known about the Pr number dependence. Our results clearly indicate that Prandtl number does not affect the transition to hard turbulence, at least in a qualitative sense. The coexistence of a large-scale circulation and small-scale thermals, proposed to be the mode of convection at high Ra[1] can be captured visually. From these 2-D calculations at infinite Prandtl number there can be no question that a L.S.C. circulation maintains a "wind,"[2] thus exerting a strong influence on the subsequent evolution of the thermals. In this connection our calculations are in full agreement with the laboratory experiments by Sano *et al.*[1] and Castaing *et al.*[2] Sirovich *et al.*[3] did not find the wind sustained over long time scales in their 3-D numerical model. In the range of Ra between 10^7 and 10^8 the mode of convection changes significantly. Most of the plumes are broken to pieces, which are then effectively mixed. This leads to a different mechanism of heat transport for this high Rayleigh number regime, which may be the cause for the transition to hard turbulence. The L.S.C. itself, or in other words, the number of L.S.C. systems, is time dependent in the case of aspect ratio 10. This finding makes the definition of global parameters such as the critical Rayleigh number or the overturn time much more problematic. However, changes of the L.S.C. operate over a much longer time scale than fluctuations due to boundary layer instabilities. Therefore, we are justified to consider the L.S.C. as being "quasistable."

The preferred aspect ratio of the individual L.S.C. systems lie between 1.5 and 4 with the tendency to increase with larger Ra. This effect, predicted by the 2-D model, has also been observed experimentally by Krishnamurti and Howard.[7] Since the heat transport efficiency depends inversely on the aspect ratio,[11,16] the predictions based on square-box, two-dimensional numerical experiments[23] are too high for realistic time-dependent systems. The combined effects of (a) increasing the aspect ratio with increasing Ra and (b) decreasing the heat transport in every individual cell by disconnection of the plumes makes the discrepancy even greater with Ra. The latter mechanism is responsible for the

This article is copyrighted as indicated in the article. Reuse of AIP content is subject to the terms at: http://scitationnew.aip.org/termsconditions. Downloaded to IP: 169.237.93.46 On: Wed, 22 Oct 2014 15:52:15

exponent in the Nu–Ra relationship to be reduced from 1/3 to a value of 0.282.[2]

In these two-dimensional calculations we found evidence for the regions: boundary layer, mixing layer, and central region, as observed in the three-dimensional laboratory experiments of Castaing *et al.*,[2] Sano *et al.*,[1] Solomon and Gollub[10] and in the numerical study by Sirovich *et al.*[3] However, the basic phenomenon of this scenario, i.e., growing thermals drifting with the L.S.C. is not an exclusive feature of hard turbulence. In fact, it can appear at much lower Ra numbers like 5×10^5 or less.[6] Under such circumstances the thermals are usually drifting almost positively with the L.S.C., until they meet stable plumes which can penetrate through the entire fluid layer. This situation changes at very high Ra where all plumes remain disconnected.

Violent plume–plume collision and outbursts from the boundary layer are the dynamical consequences of the concentrated buoyancy, leading to a temporarily connected plume, even at $\mathrm{Ra}=10^8$. During their existence these plumes can collect minor instabilities and bring them on their way up to the top boundary.[24,22] It is important to note that in the recent laboratory work of Solomon and Gollub[10] plume–plume collisions were found under three-dimensional situations. This lends some support to the physics captured by the two-dimensional simulations. At moderate Ra, the drifting and colliding instabilities mainly modulate the L.S.C. At higher Ra plume–plume collisions are necessary in order to generate those plumes, that can penetrate through the entire layer. The full richness of the dynamics defies all verbal explanations and the authors refer at this point to the video movie.

What then are the possible geodynamical implications? The style of time-dependent, multiscale convection is extremely attractive in issues related to convection in the Earth's mantle.[6] It offers the possibility to explain large-scale motions, as those associated with the motion of the large surface plates, and simultaneously anomalies with much smaller scale, like hot spots. Moreover, seismological observations[25] as well as geochemical considerations[26] give indications for strongly deflected plumes in the Earth's mantle. These deflections can be explained by the two-scale convection model in a self-consistent way. However, the transition to another different convective regime at high Ra and the related phenomenon of "broken plumes" may provide an upper bound on Ra in the mantle today. Effects of internal-heating, compressibility, depth-dependent thermodynamic parameters, and variable viscosity are other important aspects in mantle convection that must be investigated before any definite conclusions can be drawn. We still have to examine the extent to which the disconnected patches can account for the prominent regions of updwelling mantle material and the related thermal, chemical, and topographical anomalies. In the event that we cannot, then the mantle is likely to be in a Ra regime, which is below the transition to hard turbulence.

ACKNOWLEDGMENTS

We thank L. Kadanoff for sending us preprints and S. Balachandar for stimulating discussions. We thank Anne Boyd for helping us with the manuscript and Andre Malevsky for checking the numerical accuracy.

This research has been supported by German Grant No. D.F.G.E6-56/11-2 and the Innovative Research Program of NASA.

[1] M. Sano, X. Z. Wu, and A. Lichaber, Phys. Rev. A **40**, 6421 (1989).
[2] B. Castaing, G. Gunaratne, F. Heslot, L. Kadanoff, A. Libchaber, S. Thomae, X. Z. Wu, S. Zaleski, and G. Zanetti, J. Fluid Mech. **204**, 1 (1989).
[3] L. Sirovich, S. Balachandar, and M. R. Maxey, Phys. Fluids A **1**, 1911 (1989).
[4] P. Machetel and D. A. Yuen, Geophys. Res. Lett. **13**, 1470 (1986).
[5] U. R. Christensen, Geophys. Res. Lett. **14**, 220 (1987).
[6] U. Hansen and A. Ebel, Geophys. J. **94**, 181 (1988).
[7] R. Krishnamurti and L. N. Howard, Proc. Natl. Acad. Sci. USA **78**, 1981 (1981).
[8] H. J. Melosh, in *The Origin of the Earth*, edited by J. Jones and H. Newsom (Oxford U.P., New York, 1990).
[9] I. Goldhirsch, R. B. Pelz, and S. A. Orszag, J. Fluid Mech. **199**, 1 (1989).
[10] T. H. Solomon and J. P. Gollub, Phys. Rev. Lett. **64**, 2382 (1990).
[11] P. L. Olson and G. M. Corcos, Geophys. J. R. Astron. Soc. **62**, 195 (1980).
[12] B. Blankenbach, F. Busse, W. Christensen, L. Cserepes, D. Gunkel, U. Hansen, H. Harder, G. Jarvis, M. Koch, G. Marquart, D. Moore, P. Olson, H. Schmeling, and T. Schnaubelt, Geophys. Int. **98**, 23 (1989).
[13] T. J. R. Hughes, *The Finite Element Method* (Prentice–Hall, Englewood Cliffs, NJ, 1987).
[14] K.-H. Winkler, J. W. Chalmers, S. W. Hodson, P. R. Woodward, and N. J. Zabusky, Phys. Today **40**, 28 (1987).
[15] U. R. Christensen and D. A. Yuen, Geophys. Res. Lett. **15**, 577 (1988).
[16] U. Hansen and A. Ebel, Phys. Earth Planet. Int. **36**, 374 (1984).
[17] L. N. Howard in *Proceedings of the 11th International Congress of Applied Mechanics*, Munich, 1966, edited by H. Dörtler (Springer, Berlin, 1966), pp. 1109–1115.
[18] S. Balachandar (private communication, 1990).
[19] J. N. Skilbeck and J. A. Whitehead, Nature **272**, 499 (1978).
[20] M. Gurnis, Nature **332**, 695 (1988).
[21] A. V. Malevsky and D. A. Yuen, submitted to Phys. Fluids A (1990).
[22] A. P. Vincent and D. A. Yuen, Phys. Rev. A **38**, 328 (1988).
[23] U. R. Christensen, Geophys. Astrophys. Fluid Dyn. **46**, 93 (1989).
[24] S. Honda and D. A. Yuen, Earth Planet. Sci. Lett. **99**, 349 (1990).
[25] A. M. Dziewonski and J. H. Woodhouse, Science **236**, 37 (1987).
[26] M. A. Richards and R. W. Griffiths, Geophys. J. **94**, 367 (1988).

This article is copyrighted as indicated in the article. Reuse of AIP content is subject to the terms at: http://scitationnew.aip.org/termsconditions. Downloaded to IP: 169.237.93.46 On: Wed, 22 Oct 2014 15:53:15